Chinese Journal of Aeronautics, 2013,26(1): 194–200

Chinese Society of Aeronautics and Astronautics
& Beihang University

Chinese Journal of Aeronautics

cja@buaa.edu.cn
www.sciencedirect.com

A novel target detection approach based on adaptive radar waveform design

Wang Haitao *, Shi Lei, Wang Youlin, Ben De

Nanjing Research Institute of Electronics Technology, Nanjing 210039, China

Received 17 October 2011; revised 17 January 2012; accepted 23 May 2012
Available online 16 January 2013

KEYWORDS

Adaptive waveform design;
Generalized likelihood ratio test;
Multiple particle filter;
Principal component analysis;
Radar systems;
Space-based radar

Abstract To resolve problems of complicated clutter, fast-varying scenes, and low signal-clutter-ratio (SCR) in application of target detection on sea for space-based radar (SBR), a target detection approach based on adaptive waveform design is proposed in this paper. Firstly, complicated sea clutter is modeled as compound Gaussian process, and a target is modeled as some scatterers with Gaussian reflectivity. Secondly, every dwell duration of radar is divided into several sub-dwells. Regular linear frequency modulated pulses are transmitted at Sub-dwell 1, and the received signal at this sub-dwell is used to estimate clutter covariance matrices and pre-detection. Estimated matrices are updated at every following sub-dwell by multiple particle filtering to cope with fast-varying clutter scenes of SBR. Furthermore, waveform of every following sub-dwell is designed adaptively according to mean square optimization technique. Finally, principal component analysis and generalized likelihood ratio test is used for mitigation of colored interference and property of constant false alarm rate, respectively. Simulation results show that, considering configuration of SBR and condition of complicated clutter, 9 dB is reduced for SCR which reliable detection requires by this target detection approach. Therefore, the work in this paper can markedly improve radar detection performance for weak targets.

1. Introduction

Compared with airborne early warning (AEW) radar, space-based radar (SBR) has many unique advantages for wide-area surveillance and theatre defense, so people have paid more attention to this kind of SBR recently.[1–4] It is well known that SBR has long operation range and large beam footprint. Signal-clutter-ratio (SCR) is low when SBR monitors and tracks weak targets on sea.[5–7] With the development of waveform-agility techniques, it has been possible to design radar waveforms on track in real time. Some research has borne out that the technique of adaptive waveform design (AWD) can provide a new chance to the improvement of radar target detection.[8–10]

Sea clutter was assumed to be independent and identically Gaussian distributed in early research of signal process and waveform design for radar. However, if the sea state is heavy or the space resolution of the radar is high enough, the probability that spikes happen in sea clutter will increase and the Gaussian model cannot describe spiked sea clutter properly any more. Therefore, researchers proposed the compound Gaussian (CG) model of sea clutter.[11] This model has been

* Corresponding author. Tel.: +86 25 51822828.
E-mail address: enterescf1@qq.com (H. Wang).

Peer review under responsibility of Editorial Committe of CJA.

ELSEVIER Production and hosting by Elsevier

1000-9361 © 2013 CSAA & BUAA. Production and hosting by Elsevier Ltd. Open access under CC BY-NC-ND license.
http://dx.doi.org/10.1016/j.cja.2012.12.018

confirmed and applied widely. Some researchers have studied the target detection issue of constant false alarm ratio (CFAR) in strong CG sea clutter.[12–16]

In previous research, the approach of AWD discussed in Ref.[8] did not consider the factor of fast-varying scenes, so its performance would be degraded in the application of SBR. What's more, as described in their paper, the method of principal component analysis (PCA) used by that algorithm was primitive and its performance of clutter suppression was limited. The AWD approach discussed in Refs.[9,10] considered the fast-varying factor of the clutter, but it could not be tractable mathematically because it utilized the covariance matrix minimization. In addition, when the researchers studied the CFAR detection techniques in Refs.[12–16], they did not apply the AWD technique to their algorithms. From current open reports, the work discussed in this paper is the first attempt to integrate the AWD technique into target detection of SBR. The simulations show that detection performance can be improved markedly by this work.

2. Outline of target detection approach

We propose a target detection approach based on clutter statistics update, AWD, and advanced PCA in this paper to resolve problems of complicated clutter, fast-varying scenes, and low SCR in application of target detection on sea for SBR. The procedure of this approach is shown in Figs. 1 and 2. The overall block diagram of the algorithm and the detailed flow at Sub-dwell n ($n \geqslant 2$) are shown in Figs. 1 and 2, respectively. Every dwell duration of the radar is divided into several sub-dwells. The transmitting waveforms at Sub-dwell 1 are regular linear frequency modulated (LFM) pulses, and the received signal at Sub-dwell 1 is used to estimate the clutter covariance matrices. In addition, the received signal at this sub-dwell is used for pre-detection so as to find those cells to test further, whose amount equals to the amount of the following sub-dwells needed. Then, the variation of the clutter covariance for every following sub-dwell which corresponds to one single cell is predicted by the multiple particle filtering

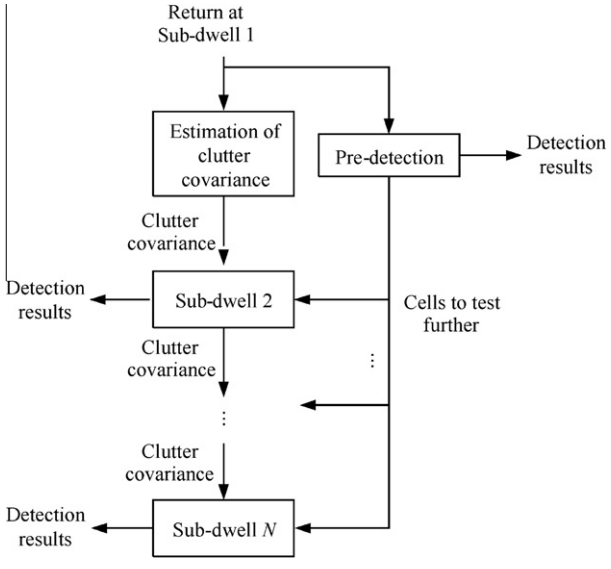

Fig. 1 Overall block diagram of algorithm based on AWD.

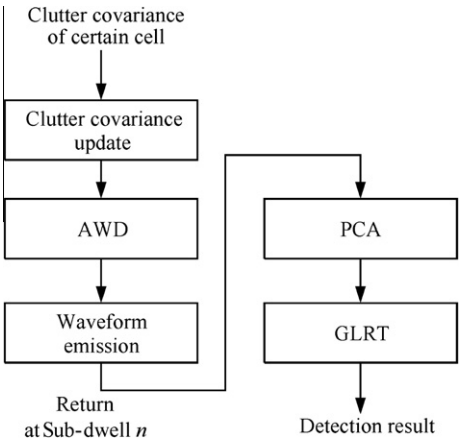

Fig. 2 Detailed flow at Sub-dwell n ($n \geqslant 2$).

(MPF) method in order to fit the fast-varying clutter and settle the problem of very large dimensionality when updating the covariance matrices.[17,18] Subsequently, the phase-modulated (PM) waveform is designed and transmitted at every following sub-dwell. The fact that we rest on to design the waveforms here is that the signal after matched filtering depends on the ambiguity function of the transmitting signal and the radar scene, and this fact leads to energy contamination among the cells. The waveforms are designed adaptively based on the texture values of the cells and mean square optimization in this paper. As a result, the contamination on the cell to test further, from other cells, can be minimized. Note that mean square optimization is much more tractable mathematically than covariance matrix minimization. At the end of every sub-dwell, the generalized likelihood ratio test (GLRT) based on PCA which projects the radar return onto the signal subspace orthogonally for the clutter elimination is utilized to gain the property of CFAR. The results of several numerical simulations on the condition of the SBR show that there is approximately 9 dB reduced for the SCR which the reliable detection (defined in Section 6) requires.

The process on every sub-dwell of the algorithm discussed above, except for Sub-dwell 1, corresponds to one of many cells to test further, so it is an algorithm which works separately. On the other hand, all the cells to test further after Sub-dwell 1 can be considered together at Sub-dwell 2 while its waveform is designed, so their detection results can be obtained at the end of Sub-dwell 2 and no more sub-dwell is needed. The version of processing together adapts to wide-area surveillance and the version of processing separately adapts to tracking task. The detection of one single target at Sub-dwell 2 will be studied in this paper as this case is the basis of the two versions.

3. Description of radar scene

If the size of a target is much larger than the wavelength of radar signal, the backscattering field of this target can be regarded as the sum of some different scatterers' contributions according to geometrical diffraction theory. We model the return of the target in the cell j as the sum of K' scatterers, and denote $\varsigma_j = [\varsigma_{j,1}\, \varsigma_{j,2} \cdots \varsigma_{j,K'}]^{\mathrm{T}}$ as the complex backscattering amplitudes vector of the target's scatterers, where $\varsigma_{j,k'}$ is the

complex amplitude of the k'th scatterer ($k' = 1,2,\cdots,K'$). The different detector based on GLRT can be obtained according to different assumptions of ς_j. We assume that ς_j is a Gaussian random vector here, and this model of target return has been used widely in the field of radar research.

Based on the compound Gaussian model, sea clutter is composed of two components, namely speckle and texture. The speckle component comes from lots of independent scattering centers reflecting the incident wave, and the texture component comes from the local average power backscattered by large ocean swells. The speckle component can be characterized by the short correlation time that is about 10 ms, and the correlation time of the texture component is much longer, which can last about 50 s in time. The texture component represents the spatial correlation that depends on the spatial resolution of the radar, the sea condition, and the wind speed. According to the compound Gaussian model, the texture value, defined as T, of every cell on sea is gamma distributed, and its probability distribution function (PDF) is

$$p(T) = \frac{2b^{v}}{\Gamma(v)} T^{2v-1} \exp(-b^2 T^2) \tag{1}$$

where the scale parameter b influences the mean of the CG distribution, and the shape parameter v represents its similarity with Gaussian distribution. The value range of v for sea clutter is usually 0.2–2, and its typical value is 0.4.

In our detection approach, every dwell time is divided into N sub-dwells, and K pulses are transmitted coherently at every sub-dwell. Let $\boldsymbol{s}_n[i]$ ($i = 0,1,\cdots,N_s - 1$) be the pulse transmitting at Sub-dwell n ($n = 0,1,\cdots,N$), where N_s is the sampling length of the pulse. It is assumed here that the pulses at all the sub-dwells have the same bandwidth and sampling length.

The radar samples the return of every sub-dwell and gains the observation $\boldsymbol{Y}_n[m,k]$, where $k = 1,2,\cdots,K$, $m = m_0, m_1, \cdots, m_{M_n-1}$, M_n is the amount of the cells in valid gate of every sub-dwell, and m_0 the number of the lowest range cell. Then, the radar return at Sub-dwell n, $\boldsymbol{Y}_n[m,k]$, can be written as

$$\boldsymbol{Y}_n[m,k] = \sum_{i=0}^{N_s} \boldsymbol{B}_n[m-i,k]\boldsymbol{s}_n[i] + \boldsymbol{V}_n[m,k] \tag{2}$$

where $\boldsymbol{V}_n[m,k]$ represents the Gaussian white noise and $\boldsymbol{B}_n[m,k]$ the complex reflectivity of the certain cell on sea.

Define the transmitting signal matrix $\boldsymbol{P}_n$ for Sub-dwell n, which is an $M_n \times N_v$ matrix and can be written as

$$\boldsymbol{P}_n = \begin{bmatrix} s_n(0) & s_n(1) & \cdots & s_n(N_s-1) & 0 & 0 & \cdots & 0 \\ 0 & s_n(0) & s_n(1) & \cdots & s_n(N_s-1) & 0 & \cdots & 0 \\ \vdots & \vdots & \vdots & \vdots & \vdots & \vdots & \vdots & \vdots \\ 0 & 0 & \cdots & \cdots & \cdots & \cdots & s_n(N_s-2) & s_n(N_s-1) \end{bmatrix} \tag{3}$$

where $N_v = N_s + M_n - 1$. We denote $\boldsymbol{B}_n[m,k]$ as the complex reflectivity of one cell on sea, which considers the kth ($k = 1,2,\cdots,K$) pulse and the mth ($m = m_0, m_1, \cdots, m_{N_v-1}$) range cell, so the backscattering situation of the sea in the view field of the radar can be represented as the backscattering reflectivity matrix $\boldsymbol{B}_n$. $\boldsymbol{B}_n$ is an $N_v \times K$ matrix whose element is $\boldsymbol{B}_n[m,k]$, with range (fast time) increasing down along the columns and transmitted pulse (slow time) increasing rightward across the rows.

We process $\boldsymbol{B}_n$ across every row by discrete Fourier transform (DFT) and obtain the elements of the scattering matrix $\boldsymbol{A}_n$:

$$\boldsymbol{A}_n[m,l] = \frac{1}{\sqrt{K}} \sum_{k=1}^{K} \boldsymbol{B}_n[m,k] \mathrm{e}^{-\mathrm{j}2\pi kl/K} \tag{4}$$

where $l \in \{-(K-1)/2,\ -(K-2)/2, \cdots, (K-1)/2\}$. The relationship between $\boldsymbol{A}_n$ and $\boldsymbol{B}_n$ is shown in Eq. (5):

$$\boldsymbol{A}_n = \boldsymbol{B}_n \boldsymbol{D} \tag{5}$$

where $\boldsymbol{D}$ is the so-called DFT matrix. $\boldsymbol{A}_n$ is the range-Doppler expression of the matrix $\boldsymbol{B}_n$. Assuming that K is odd, the middle column of $\boldsymbol{A}_n$ expresses static scatterers, its former $(K-1)/2$ columns express those scatterers that have negative Doppler frequency shifts, and its latter $(K-1)/2$ columns express those scatterers that have positive Doppler frequency shifts.

Considering the transmitting signal matrix $\boldsymbol{P}_n$ and Eq. (2), we get the observation matrix $\boldsymbol{Y}_n$ that is an $M_n \times K$ matrix by Eq. (6):

$$\boldsymbol{Y}_n = \boldsymbol{P}_n \boldsymbol{B}_n + \boldsymbol{V}_n \tag{6}$$

where $\boldsymbol{V}_n$ is the noise matrix at Sub-dwell n which is an $M_n \times K$ matrix too. The element of $\boldsymbol{V}_n$ is written as $\boldsymbol{V}_n[m,k]$.

The scatterers on the ground will travel with respect to the radar platform when a SBR works. Some scatterers will move out of the valid gate, and some others will move into it. In order to describe the evolution of scattering matrix in fast-varying scenes, we introduce an evolutionary matrix $\boldsymbol{F}$ to represent the movement of the scatterers. The backscattering reflectivity of the new cells that move into the valid gate can be represented as the weighted exponential sum of the reflectivity of the close neighbor cells which have the same Doppler frequency.[10] The movement of the scatterers happens in every column of $\boldsymbol{A}_n$ until all the empty cells have new scatterers. We stack all the columns of the matrix $\boldsymbol{A}_n$ from left to right to form a vector $\boldsymbol{a}_n$ with a length of KN_v. This vectorized operation is represented as $\boldsymbol{a}_n = \mathrm{vec}(\boldsymbol{A}_n)$, and the evolution of the vectorized scattering matrix is given as

$$\boldsymbol{a}_n = \boldsymbol{F}\boldsymbol{a}_{n-1} + \boldsymbol{w}_n \tag{7}$$

where $\boldsymbol{w}_n$ is the zero mean Gaussian noise vector with the covariance $\boldsymbol{R}_{\mathrm{Cov\_}\boldsymbol{w}_n}$. $\boldsymbol{F}$ is a $KN_v \times KN_v$ block-diagonal matrix which represents the movement of the scatterers between sub-dwells. The observation matrix $\boldsymbol{Y}_n = \boldsymbol{P}_n\boldsymbol{A}_n\boldsymbol{D}^{-1} + \boldsymbol{V}_n$. Considering the matrix relationship $\mathrm{vec}(\boldsymbol{GZL}) = (\boldsymbol{L}^{\mathrm{H}} \otimes \boldsymbol{G})\boldsymbol{z}$, where $\boldsymbol{G}$, $\boldsymbol{Z}$, and $\boldsymbol{L}$ are three arbitrary matrices, $\boldsymbol{z} = \mathrm{vec}(\boldsymbol{Z})$, $\otimes$ represents Kronecker product, the superscript "H" expresses Hermitian operation we express the vectorized observation as the following formula:

$$\boldsymbol{y}_n = (\boldsymbol{D}^{-\mathrm{H}} \otimes \boldsymbol{P}_n)\boldsymbol{a}_n + \boldsymbol{v}_n = \breve{\boldsymbol{P}}_n \boldsymbol{a}_n + \boldsymbol{v}_n \tag{8}$$

where $\boldsymbol{y}_n = \mathrm{vec}(\boldsymbol{Y}_n)$, $\breve{\boldsymbol{P}}_n = \boldsymbol{D}^{-\mathrm{H}} \otimes \boldsymbol{P}_n$. $\boldsymbol{a}_n$ in Eqs. (7) and (8) is unknown.

4. Update of sea clutter statistic

The clutter covariance matrices of the cells to test further are estimated at Sub-dwell 1 based on its return data. Therefore, it is a key point to update these covariance matrices according to the movement of the radar platform.

Let $\boldsymbol{R}_{\mathrm{Cov\_}\boldsymbol{a}_n}$ be the covariance matrix of $\boldsymbol{a}_n$, and according to the dynamic model shown in Eq. (7), there is

$$\boldsymbol{R}_{\mathrm{Cov\_}\boldsymbol{a}_n} = E\left(\boldsymbol{a}_n\boldsymbol{a}_n^{\mathrm{H}}\right) = \boldsymbol{F}\boldsymbol{R}_{\mathrm{Cov\_}\boldsymbol{a}_{n-1}}\boldsymbol{F}^{\mathrm{H}} + \boldsymbol{R}_{\mathrm{Cov\_}\boldsymbol{w}_n} \tag{9}$$

where $\boldsymbol{R}_{\mathrm{Cov\_}\boldsymbol{w}_n}$ is the covariance matrix of $\boldsymbol{w}_n$. Similarly, for the covariance matrix of vectorized observation in Eq. (8), there is

$$\boldsymbol{R}_{\mathrm{Cov\_}\boldsymbol{y}_n} = \breve{\boldsymbol{P}}_n\boldsymbol{R}_{\mathrm{Cov\_}\boldsymbol{a}_n}\breve{\boldsymbol{P}}_n^{\mathrm{H}} + \boldsymbol{R}_{\mathrm{Cov\_}\boldsymbol{v}_n} \tag{10}$$

where $\boldsymbol{R}_{\mathrm{Cov\_}\boldsymbol{v}_n}$ is the covariance matrix of $\boldsymbol{v}_n$. We can get $p(\boldsymbol{y}_n|\boldsymbol{R}_{\mathrm{Cov\_}\boldsymbol{a}_n})$ to update the filter using Eq. (10).[10] Note that $\boldsymbol{R}_{\mathrm{Cov\_}\boldsymbol{w}_n}$ in Eq. (9) and $\boldsymbol{R}_{\mathrm{Cov\_}\boldsymbol{v}_n}$ in Eq. (10) ought to be Wishart distributed because they are the covariance matrices of the multivariate normal samples $\boldsymbol{w}_n$ and $\boldsymbol{v}_n$, respectively.

Particle filtering (PF) is a sequential Monte-Carlo method which approximates a probability density function by sampling. It can approximate Kalman filtering well even if the system model is non-linear or non-Gaussian. However, lots of particles will be needed and the computation complexity will be unacceptable when the dimensionality of the state space is too large, as in our case here. There is the relationship as Eq. (5) between $\boldsymbol{A}_n$ and $\boldsymbol{B}_n$. Once $\boldsymbol{R}_{\mathrm{Cov\_}\boldsymbol{a}_n}$ is estimated, we can get $\boldsymbol{R}_{\mathrm{Cov\_}\boldsymbol{b}_n} = (\boldsymbol{D}\otimes\boldsymbol{I}_{N_v})\boldsymbol{R}_{\mathrm{Cov\_}\boldsymbol{a}_n}(\boldsymbol{D}^{\mathrm{H}}\otimes\boldsymbol{I}_{N_v})$. Let $\boldsymbol{\alpha}_n = f_n(\boldsymbol{\alpha}_{n-1},\boldsymbol{\omega}_{n-1})$ and $\boldsymbol{\beta}_n = h_n(\boldsymbol{\alpha}_n,\boldsymbol{\gamma}_n)$ be the dynamic equation and the measurement equation, respectively. $\boldsymbol{\alpha}_n$ is a high-dimensional system state vector at time step n. f_n and h_n are two certain functions (nonlinear probably). $\boldsymbol{\omega}_n$ and $\boldsymbol{\gamma}_n$ are the random vectors. Let $\boldsymbol{\alpha}_n$ be divided into sub-vectors, that is $\boldsymbol{\alpha}_n = [\boldsymbol{\alpha}_{1,n}^{\mathrm{T}}\ \boldsymbol{\alpha}_{2,n}^{\mathrm{T}}\ \cdots\ \boldsymbol{\alpha}_{L,n}^{\mathrm{T}}]^{\mathrm{T}}$, and $\boldsymbol{\alpha}_{l,n}^{\mathrm{T}}(l = 1,2,\cdots,L)$ is estimated by a certain PF. This is the so-called multiple particle filter. At the time step n, L PFs are working simultaneously and the state vector $\boldsymbol{\alpha}_n$ is composed eventually.

In order to solve the system equation using the Bayesian technique, we vectorize the dynamic model of Eq. (9) and the observation model of Eq. (10) as follows:

$$\begin{cases} \boldsymbol{r}_{\mathrm{Cov\_}\boldsymbol{a}_n} = (\boldsymbol{F}\otimes\boldsymbol{F})\boldsymbol{r}_{\mathrm{Cov\_}\boldsymbol{a}_{n-1}} + \boldsymbol{r}_{\mathrm{Cov\_}\boldsymbol{w}_n} \\ \boldsymbol{r}_{\mathrm{Cov\_}\boldsymbol{y}_n} = (\breve{\boldsymbol{P}}_n\otimes\breve{\boldsymbol{P}}_n)\boldsymbol{r}_{\mathrm{Cov\_}\boldsymbol{a}_n} + \boldsymbol{r}_{\mathrm{Cov\_}\boldsymbol{v}_n} \end{cases} \tag{11}$$

where $\boldsymbol{r}_{\mathrm{Cov\_}\boldsymbol{a}_n} = \mathrm{vec}(\boldsymbol{R}_{\mathrm{Cov\_}\boldsymbol{a}_n})$,$\boldsymbol{r}_{\mathrm{Cov\_}\boldsymbol{y}_n} = \mathrm{vec}(\boldsymbol{R}_{\mathrm{Cov\_}\boldsymbol{y}_n})$,$\boldsymbol{r}_{\mathrm{Cov\_}\boldsymbol{v}_n} = \mathrm{vec}(\boldsymbol{R}_{\mathrm{Cov\_}\boldsymbol{v}_n})$ and $\boldsymbol{r}_{\mathrm{Cov\_}\boldsymbol{w}_n} = \mathrm{vec}(\boldsymbol{R}_{\mathrm{Cov\_}\boldsymbol{w}_n})$. The length of $\boldsymbol{r}_{\mathrm{Cov\_}\boldsymbol{a}_n}$ is $(KN_v)^2$, so its dimensionality will be very large even if a small amount of pulses are used. Such a high dimensionality will make PF or Kalman filter hard to handle even if the transform is linear, and the use of MPF will be necessary.

$\boldsymbol{F}\otimes\boldsymbol{F}$ in Eq. (11) is block-diagonal, that is

$$\boldsymbol{F}\otimes\boldsymbol{F} = \begin{bmatrix} \boldsymbol{F}_1\otimes\boldsymbol{F} & 0 & \cdots & 0 \\ 0 & \boldsymbol{F}_2\otimes\boldsymbol{F} & \cdots & 0 \\ \vdots & \vdots & & \vdots \\ 0 & 0 & \cdots & \boldsymbol{F}_K\otimes\boldsymbol{F} \end{bmatrix} \tag{12}$$

where $\boldsymbol{F}_k$ is the kth block matrix on the diagonal line of $\boldsymbol{F}(k = 1,2,\cdots,K)$. Based on the structure of $\boldsymbol{F}\otimes\boldsymbol{F}$, the variation of the state vector can be divided into K independent sub-systems:

$$\boldsymbol{r}_{\mathrm{Cov\_}\boldsymbol{a}_n} = \begin{bmatrix} \boldsymbol{\Lambda}_{1,n}^{\mathrm{T}} & \boldsymbol{\Lambda}_{2,n}^{\mathrm{T}} & \cdots & \boldsymbol{\Lambda}_{K,n}^{\mathrm{T}} \end{bmatrix}^{\mathrm{T}} \tag{13}$$

where the dimensionality of every sub-vector $\boldsymbol{\Lambda}_{k,n}^{\mathrm{T}}(k = 1,2,\cdots,K)$ is KN_v^2. K PFs are used, and every filter corresponds to a sub-system. We use the following dynamic and measurement models to estimate the kth sub-system:

$$\begin{cases} \boldsymbol{\Lambda}_{k,n} = (\boldsymbol{F}_k\otimes\boldsymbol{F})\boldsymbol{\Lambda}_{k,n-1} + \boldsymbol{r}_{k,\mathrm{Cov\_}\boldsymbol{w}_n} \\ \boldsymbol{r}_{\mathrm{Cov\_}\boldsymbol{y}_n} = (\breve{\boldsymbol{P}}_n\otimes\breve{\boldsymbol{P}}_n)\boldsymbol{r}_{\mathrm{Cov\_}\boldsymbol{a}_n} + \boldsymbol{r}_{\mathrm{Cov\_}\boldsymbol{v}_n} \end{cases} \tag{14}$$

The detailed update method of every PF's weight can be found in Refs.[17,18].

5. Waveform design

After Sub-dwell 1, it is assumed that we have determined to access the range-Doppler cell j at Sub-dwell 2. As discussed before, all the range-Doppler cells contribute clutter energy to the return of the cell j after matched filtering. We design the waveform $\boldsymbol{s}_2[n]$ for Sub-dwell 2, whose auto-correlation function (ACF) is close to zero at the cells having high clutter energy, to minimize clutter energy contamination to the test cell.

Let $s_2(t)$ be unimodular phase-modulated waveform, which is expressed as

$$s_2(t) = \exp(\mathrm{j}\phi(t)), \quad 0 \leqslant t \leqslant T_{\mathrm{s}} \tag{15}$$

where $\phi(t)$ is expanded in terms of an orthogonal set of basis functions $\varphi_i(t)$ as

$$\phi(t) = \sum_{i=1}^{N_{\mathrm{s}}}\lambda_i\phi_i(t) \tag{16}$$

where

$$\varphi_i(t) = \begin{cases} 1, & (i-1)\Delta T \leqslant t \leqslant i\Delta T \\ 0, & \text{Otherwise} \end{cases}$$

where $i = 1,2,\cdots,N_{\mathrm{s}}$. The total waveform duration $T_{\mathrm{s}} = N_{\mathrm{s}}\Delta T$. As discussed before, we assume that the waveforms of all the sub-dwells have the same sampling length and bandwidth. The PM waveform shown in Eq. (15) is obtained easily, and this kind of waveform can utilize the transmitting power of radar fully as it is not amplitude-modulated.

Define ACF of $s_2(t)$ as

$$z_{s_2}(\tau,\omega) = \int_{-\infty}^{\infty}\int_{-\infty}^{\infty} s_2(t,f)s_2^*(t-\tau,f-\omega)\mathrm{d}\omega\mathrm{d}\tau \tag{17}$$

and then it is a key point to determine the coefficient λ_i in Eq. (16) for minimizing the following formula:

$$J(\boldsymbol{\lambda}) = \int_{Z_{\tau,\omega}} |z_{s_2}(\tau,\omega)|^2\mathrm{d}\tau \tag{18}$$

where $\boldsymbol{\lambda} = [\lambda_1\ \lambda_2\ \cdots\ \lambda_{N_{\mathrm{s}}}]^{\mathrm{T}}$ and $Z_{\tau,\omega}$ is the set of the cells which have large texture values. Essentially, the adaptive waveform design we talk about here is to synthesize PM signal whose ACF approximates the special function well in the sense of mean square.

The ACF of the PM waveform shown as Eq. (17) has more simple expression.[8] Using the squared magnitude of $z_{s_2}(\tau,\omega)$, the gradient and Hessian of $J(\boldsymbol{k})$ can be computed. Then the minimization of Eq. (18) can be realized by the Newton–Raphson method. This is the so-called mean square optimization, and the more details of this optimization technique can be seen in Ref.[8]. Therefore, the ACF magnitudes of the cells having large texture values are minimized with respect to the test cell. The set $Z_{\tau,\omega}$ in Eq. (18) are composed by the N_{t} cells having large texture components. As this set is discreet, the integral in Eq. (18) can be simplified to the sum operation:

$$J(\boldsymbol{\lambda}) = \sum_{Z_{\tau,\omega}} |z_{s_2}[m,n]|^2 \tag{19}$$

where the elements of $Z_{\tau,\omega}$ are the integral multiples of the sampling interval ΔT_s and the Doppler filter spacing Δf.

We have discussed the waveform design method at Sub-dwell 2, and the method at the following sub-dwells is the same.

6. Generalized likelihood ratio test

At the end of Sub-dwell n ($n \geqslant 2$), we should detect whether there is a target in the certain cell or not. Especially, we need to make a pre-detection at Sub-dwell 1 to determine the cells to test further. A GLRT based on PCA is introduced to realize the property of CFAR in this section. This detection method is applied to the returns of all the sub-dwells, and two thresholds Th1 and Th2 will be set at Sub-dwell 1 according to two different combinations of the false alarm probabilities and the detection probabilities, respectively, namely $P_{\text{fa}} = 10^{-6}/P_{\text{d}} = 0.9$ (the reliable detection) and $P_{\text{fa}} = 10^{-4}/P_{\text{d}} = 0.5$ (the critical detection) where P_{d} represents the detection probability and P_{fa} the false alarm probability. At Sub-dwell 1, we will consider that one target exists in some certain cells if their test statistics are beyond Th1, and the cells whose test statistics lie between Th1 and Th2 will be considered to test further. At the following sub-dwells, Th1 is used to check if there is a target or not in the certain test cell.

The hypothesis H_0 and H_1 are defined to express the cases that there is only clutter energy in the return of the certain cell and that there is energy of both clutter and a target in it, respectively. The detector will have CFAR property when its detection threshold is independent of clutter power. The detection threshold is usually in term of clutter covariance matrix in the research of adaptive detection. In fact, we can form the generalized likelihood ratio test independent of clutter texture component and obtain the adaptive detector. The threshold of this detector depends on the target steering matrix, more accurately, on the rank of the target steering matrix (namely the size of signal subspace).[15] For the Gaussian scatterer model of a target, the log-likelihood-ratio $\ln \boldsymbol{\Theta}(\tilde{\boldsymbol{r}}_j)$ of this detector can be written as

$$\ln \boldsymbol{\Theta}(\tilde{\boldsymbol{r}}_j) = -K \ln K - \ln\left((K-K')\frac{\tilde{\boldsymbol{r}}_j^{\text{H}} \widetilde{\boldsymbol{Q}}_j \tilde{\boldsymbol{r}}_j}{\tilde{\boldsymbol{r}}_j^{\text{H}} \widetilde{\boldsymbol{Q}}_j^{\perp} \tilde{\boldsymbol{r}}_j} - (K'-1)\right) + K \ln\left(1 + \frac{\tilde{\boldsymbol{r}}_j^{\text{H}} \widetilde{\boldsymbol{Q}}_j \tilde{\boldsymbol{r}}_j}{\tilde{\boldsymbol{r}}_j^{\text{H}} \widetilde{\boldsymbol{Q}}_j^{\perp} \tilde{\boldsymbol{r}}_j}\right) \tag{20}$$

where K' is the size of the signal subspace, $\boldsymbol{r}_j$ the return of the cell j, and the matrix $\boldsymbol{Q}_j$ the orthogonal projector onto the signal subspace. $\tilde{\boldsymbol{r}}_j$ and $\widetilde{\boldsymbol{Q}}_j$ are obtained by whitening $\boldsymbol{r}_j$ and $\boldsymbol{Q}_j$, and $\widetilde{\boldsymbol{Q}}_j^{\perp} = \boldsymbol{I} - \widetilde{\boldsymbol{Q}}_j$ which is the orthogonal projector onto the clutter subspace. Note that the signal and clutter subspaces are independent of the waveform variation.[8] The threshold of this GLRT based on the Gaussian scatterers model is difficult to derive in a closed form, so we resort to the Monte-Carlo method to compute it.

The orthogonal projector onto the signal subspace can be derived by the clutter covariance matrix and the target steering matrix. In order to estimate the steering matrix, we shall restrict this matrix to the structure of the signal subspace first. That is to say, we should estimate the Doppler frequencies of the target scatterers by the super resolution method. The method that uses the eigen-decomposition to analyze the signal subspace is sensitive to the estimation error, especially in the case of the small-size observation vector. Therefore, we may use root-MUSIC (Multiple Signal Classification) or estimation signal parameters via rotational invariance techniques (ESPRIT) algorithm which does not maximize the MUSIC pseudo-spectrum but estimates the Doppler frequency directly. The size of the signal subspace, which is the K' mentioned in Section 3, ought to be known previously, but this knowledge is not apriori known and needs to be estimated. The size of the signal subspace equals to the amount of the eigen-values which are larger than the minimum eigen-values of the covariance matrix of the observation. However, the estimation of the covariance matrix is usually not precise, so the size of the signal subspace cannot be obtained by counting the eigen-values. As a result, we shall resort to some criterions based on the information theory, such as the Akaike information criterion (AIC) and minimum description length (MDL). AIC prefers to overestimate the size of signal subspace even if SCR is high. MDL may underestimate it when K is small or SCR is low. The estimation of the signal subspace size remains a tricky issue.

7. Simulation results

We introduce one simple example first to illustrate the validity of AWD based on the mean square optimization shown in Section 5. In this example, there is one single target and it is detected reliably at Sub-dwell 2. The radar platform is assumed to be fixed, so the clutter covariance need not be updated. What's more, we only carry out matched filtering along the range direction and detect the target, so the autocorrelation function Eq. (17) in Section 5 can be degraded to a single-argument function with respect to the time lag. The CG sea clutter is generated by the method of spherically invariant random process (SIRP), and the shape parameter of the CG clutter is set as 0.4. The range of the test cell is 10 km away, and the operation frequency is 10 GHz. The amount of the pulses transmitting at each of the two sub-dwells is 10, the duration time of the pulses is 1.5 μs, and the pulse repeat interval (PRI) is 100 μs. The duration time of the two sub-dwells is both 1 ms. Assume that the sampling rate is 100 MHz, so there are 150 samples in one pulse. The waveform $s_1(n)$ transmitting at Sub-dwell 1 is the regular LFM pulse, and the waveform $s_2(n)$ designed for Sub-dwell 2 has the same pulse width and bandwidth as the waveform at Sub-dwell 1. There are $N_s = 150$ phase functions being used in Eq. (16). We estimate the texture of all the cells, and choose $N_t = 140$ cells having larger texture to optimize the ACF of $s_2(n)$. The result of waveform design is shown in Fig. 3. For comparison, there are the ACF magnitudes of the regular LFM waveform and that of the designed waveform in this figure, which are shown as the solid line and the dashed line, respectively. In Fig. 3, the lags of the 140 cells having larger texture are labeled with asterisks. It can be seen that the ACF amplitudes of the designed waveform on these 140 lags are small indeed. Some ACF side-lobes of the designed waveform are higher than that of LFM waveform, but the clutter corresponding to these side-lobes is weak and their effect is small.

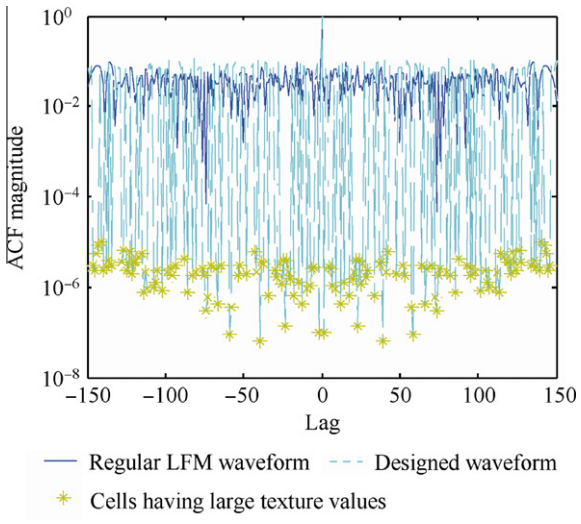

Fig. 3 ACF comparison of designed PM waveform with LFM chirp.

Subsequently, we simulate the clutter of the SBR by the way discussed in Ref.[7] and analyze the performance of the detection approach. The main parameters of the SBR candidate are shown in Table 1, and the detailed description of the SBR can be found in Refs.[5,6]. While there were 32 pulses processed coherently in these two references, the amount of pulses in one sub-dwell, namely the amount of the pulses processed coherently, is set to 16 here. In a similar way to the preceding example, we only study the detection problem of one single weak target which is modeled as some Gaussian scatterers, and one dwell duration is composed by two sub-dwells. We assume that the shape parameter of the CG clutter is 0.4, and the receiver operating curves (ROCs) of four different detection approaches for the reliable detection is shown in Fig. 4, which are:

Case 1: The ROC obtained by the approach discussed in this paper is shown as the dashed line.

Case 2: The ROC obtained by the approach discussed in this paper, without clutter covariance matrix updating at Sub-dwell 2 as discussed in Section 4, is shown as the dotted line.

Case 3: The ROC obtained by the approach discussed in this paper, without AWD at Sub-dwell 2 as discussed in Section 5, is shown as the dot-dashed line.

Case 4: The ROC obtained by processing 32 regular LMF pulses coherently, i.e., not dividing the dwell duration but detecting as discussed in Section 6, is shown as the solid line.

Table 1 Parameters of SBR candidate.

Parameter	Value
Center frequency (GHz)	1.25
PRI (μs)	500
Pulse width (μs)	100
Bandwidth (MHz)	10
Antenna length (m)	50.0
Antenna height (m)	2.10

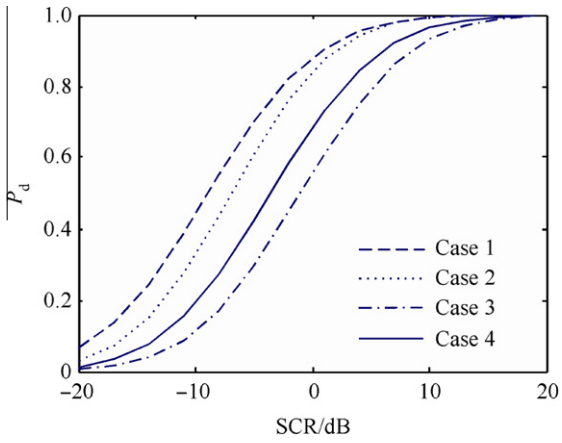

Fig. 4 Detection performance comparison of four different detection approaches.

In Fig. 4, compared with the approach that 16 regular LFM pulses are processed coherently (Case 3), the SCR which the reliable detection needs can decrease approximately 9 dB by the complete approach discussed in this paper (Case 1). Compared with the approach that 32 pulses are processed coherently (Case 4), the SCR which the reliable detection needs can decrease approximately 6 dB by the complete approach discussed in this paper (Case 1). Compared with the approach without clutter covariance matrix update (Case 2), the SCR which the reliable detection needs can decrease about 3 dB by the complete approach discussed in this paper (Case 1).

Finally, based on the SBR configuration of the above simulation, we change the shape parameter of the CG sea clutter and verify the performance of this detection approach further. The ROCs on the condition that the shape parameters of the clutter are 0.2, 0.4, and 2 are shown as the dashed line, the solid line, and the dot-dashed line in Fig. 5, respectively. It can be seen that the SCR for the reliable detection will fall between −5 and 5 dB when the shape parameter falls between 0.2 and 2.

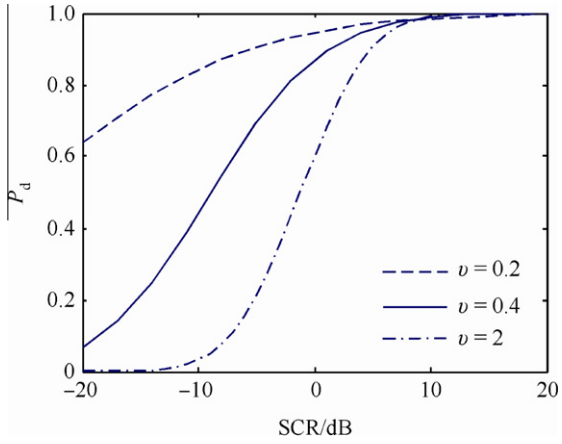

Fig. 5 Detection performance comparison for clutter with different shape parameters.

8. Conclusions

A novel algorithm based on adaptive waveform design is proposed for SBR in this paper, by which targets can be detected effectively in complicated heavy fast-varying sea clutter. We carry out three simulation experiments, and the results show that: (1) the contribution of clutter energy to the test cell, from other cells having large texture, can be reduced by the method of AWD discussed in this paper; (2) the SCR for the reliable detection can improve 9 dB by the detection approach proposed in this paper on the condition of the spiked sea clutter and the SBR configuration compared with the traditional approach of transmitting the regular LFM burst, and the dynamic update of clutter covariance matrix can offer SCR improvement of 2–3 dB; (3) this detection algorithm has better performance in more spiked clutter scenes. In future, we will introduce the schedule of multiple antennas and channels to our research, which has more degrees of freedom and is expected to implement the surveillance and tracking task for SBR better.

Acknowledgments

This work was supported by the National Defense Pre-Research Foundation of China. The authors would like to thank all the reviewers for careful and detailed revisions that helped to improve this paper.

References

1. Ben D, Lin YQ. Space-based surveillance radar. *Modern Radar* 2005;**27**(4):1–4 [Chinese].
2. Wang HT, Zhu GC, Ben D, Pan MH, Xu T, Zhang XF. A signal process algorithm for space-based radar based on past-CPIs data cube. *J Astronaut* 2008;**29**(2):275–9 [Chinese].
3. Pillai SU, Himed B, Li KY. Effect of earth's rotation and range foldover on space-based radar performance. *IEEE Trans Aerospace Electron Syst* 2006;**42**(3):917–32.
4. Wang HT, Zhu GC, Ben D, Pan MH, Yu WZ. Signal process algorithm for space-based radar based on colored-loading. *J Nanjing Univ Aeronaut Astronaut* 2008;**40**(5):651–4 [Chinese].
5. Zulch P, Davis M, Maher J, Hancock R, Theis S, Mckay J. Beam-space signal processing and analysis of a LEO L-band GMTI SBR. In: *2004 IEEE aerospace conference proceeding*; 2004.
6. Zhang YH, Hajjari A, Adzima L, Himed B. Application of beam domain STAP techniques to space-based radars. In: *Proceedings of the 36th southeastern symposium on system theory*; 2004. p. 112–6.
7. Mangiat S, Li KY, Unnikrishna PS, Himed B. Effect of terrain modeling and internal clutter motion on space based radar performance. In: *IEEE international radar conference*; 2006. p. 310–7.
8. Sira SP, Cochran D, Papandreou-Suppappola A, Morrell D, Moran W, Howard SD, et al. Adaptive waveform design for improved detection of low-RCS targets in heavy sea clutter. *IEEE J Selected Top Signal Process* 2007;**1**(1):56–66.
9. Li Y, Moran W, Sira SP, Papandreou-Suppappola A, Morrell D. Adaptive waveform design in rapidly-varying radar scenes. In: *2009 international waveform diversity and design conference*; 2009. p. 263–7.
10. Li Y, Sira SP, Moran B, Suvorova S, Cochran D, Morrell D, et al. Adaptive sensing of dynamic target state in heavy sea clutter. In: *CAMPSAP 2007*; 2007. p. 9–12.
11. Watts S. Performance measures for airborne maritime surveillance radars. In: *IEE Colloguium on Specifying and Measuring Performance of Modern Radar Systems*; 1998. p. 1–6.
12. Li J, Wang XS, Wang T. GLRT detectors for aircraft wake vortices in clear air. *Chin J Aeronaut* 2010;**23**(6):698–706.
13. Bandiera F, Besson O, Ricci G. Adaptive detection of distributed targets in compound-Gaussian noise without secondary data: a Bayesian approach. *IEEE Trans Signal Process* 2011;**59**(12): 5698–708.
14. Roy LP, Kumar RVR. A GLRT detector in partially correlated texture based on compound-Gaussian clutter. In: *2010 national conference on communications*; 2010. p. 295–9.
15. Bon N, Khenchaf A, Garello R. GLRT subspace detection for range and Doppler distributed targets. *IEEE Trans Aerospace Electron Syst* 2008;**44**(2):678–96.
16. Jian T, He Y, Su F, Qu CW, Gu XF. A novel adaptive radar target detector for non-Gaussian clutter. *Acta Aeronaut Astronaut Sin* 2010;**31**(3):579–86 [Chinese].
17. Arulampalam MS, Maskell S, Gordan N, Clapp T. A tutorial on particle filters for online nonlinear/non-Gaussian Bayesian tracking. *IEEE Trans Signal Process* 2002;**50**(2):174–88.
18. Bugallo MF, Lu T, Djuric PM. Target tracking by multiple particle filtering. In: *2007 IEEE aerospace conference*; 2007. p. 1–7.

Wang Haitao received Ph.D. degree from Nanjing University of Aeronautics and Astronautics in 2008, and then became a senior engineer at Nanjing Research Institute of Electronic Technology. His main research interest is the design of space based radar.